A&A 488, 1079–1084 (2008)
DOI: 10.1051/0004-6361:20079217

Astronomy & Astrophysics

Solar atmospheric model over a highly polarized 17 GHz active region

C. L. Selhorst[1], A. Silva-Válio[1], and J. E. R. Costa[2]

[1] CRAAM, Universidade Presbiteriana Mackenzie, São Paulo, SP 01302-907, Brazil
e-mail: caius@craam.mackenzie.br
[2] DAS, Instituto Nacional de Pesquisas Espaciais, São José dos Campos, SP 12201-970, Brazil

Received 7 December 2007 / Accepted 31 May 2008

ABSTRACT

Aims. We construct a 3D solar atmospheric model to reproduce active region brightness temperature of radio observations.
Methods. A 3D solar atmospheric model was developed to reproduce the radio observations at 17 and 34 GHz from the Nobeyama Radioheliograph. The model included bremsstrahlung and gyro-resonance emission mechanisms. Both potential and force-free magnetic field extrapolations from MDI magnetograms are considered, as well as the changes in the quiet Sun atmosphere (density and temperature distributions) due to the magnetic field interaction. We analyze a highly polarized active region at 17 GHz (85 ± 5% LHCP) observed 2002 June 25 (NOAA 10008).
Results. Modeling of this region requires that the whole projected region between the magnetic field footpoints changes its atmospheric density and temperature constitution. The modeling at 17 GHz showed the following results: a) the intensity of the corrected MDI magnetograms is able to account for the emission as gyro-resonance, but, the problem with saturation points still persists; b) for a low number of saturation points, a simple linear correction can change the maximum brightness temperature results in the simulations completely; c) the brightness temperature maxima resulting from the linear correction in the magnetic field intensities reproduced all maxima observed during the day ($1.14–1.76 \times 10^5$ K); and d) the spatial brightness distribution of the gyro-resonance emission of NOAA 10008 was well-reproduced either by a potential or force-free field extrapolation with low positive α ($0.70–1.10 \times 10^{-2}$ Mm^{-1}). At 34 GHz, the emission was successfully modeled as completely free-free radiation with a brightness temperature maximum in agreement with the observations.
Conclusions. In summary the model is able to account for the observations at both frequencies, which are, however, produced by distinct emission mechanisms.

Key words. Sun: atmosphere – Sun: magnetic fields – Sun: radio radiation

1. Introduction

The development of solar dedicated instruments with high angular resolution, together with advances in computational science, provides the solar physics research with an excellent opportunity to improve knowledge of the structure of the Sun. Specifically, the Nobeyama Radioheliograph (NoRH, Nakajima et al. 1994) has constituted a noteworthy instrument to study chromospheric and low corona features at 17 GHz since 1992, and 34 GHz after 1996, with good angular resolution.

Many authors (Shibasaki et al. 1994; White et al. 1995; Kundu et al. 2001; Vourlidas et al. 2006) have studied gyro-resonance emission at radio frequencies in order to estimate the coronal magnetic field intensities. Their main results are:

- quiescent radio emission originates in the gyro-frequency first harmonics (2–4);
- gyro-resonance emission for radio frequencies above ~10 GHz are produced in regions of magnetic fields with intensities of kG;
- these magnetic fields intensities are located close to the transition region.

Vourlidas et al. (2006) made a statistical study of gyro-resonance emission at 17 GHz concluding that active regions with a degree of polarization greater than about 30% have a core of gyro-resonance emission above them. Moreover, the authors found that the lower limit for the magnetic field intensity to produce this emission is 2200 G at the photospheric level.

In a previous work Selhorst et al. (2005b) developed an atmospheric model (hereafter referred to as the SSC model), which simultaneously reproduces the brightness temperature at disk center for radio frequencies ranging from 1.4 to 400 GHz, and radius and limb brightening observations at 17 GHz.

Selhorst et al. (2005a) presented a previous 3D atmospheric model of an unpolarized active region based on the SSC model in order to fit the observations at 17 GHz. The active region observed by NoRH had degree of polarization smaller than <10% and brightness temperature maximum, $T_{B_{\max}}$, of 5.2×10^4 K. In this case only the thermal bremsstrahlung emission needed to be taken into account to fit the observations. Here we improved and tested the model for a highly lefthand-polarized active region observed at 17 GHz, where the electronic gyro-resonance is the main emission mechanism.

In this scenario, the magnetic field plays an important role, not only for gyro-resonance emission but also for generating changes in the plasma density and temperature distributions within the magnetic loops. Since current measurements of magnetic field intensities in the solar atmosphere above the photosphere are not possible, magnetic field extrapolations from photospheric magnetograms have been used to estimate and reconstruct the magnetic field in the solar atmosphere

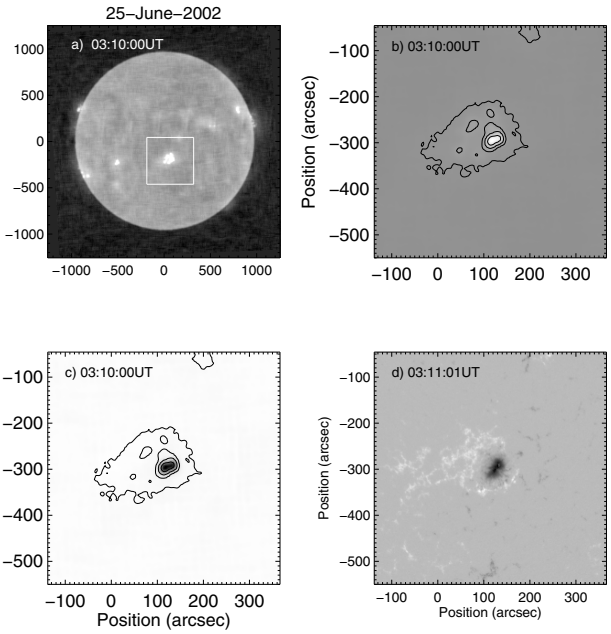

Fig. 1. a) Full-Sun radio map at 17 GHz showing the selected active region within the box. **b)** Active region with brightness temperature contours of 1.3, 2.5, 5.0, and 10.0×10^4 K. **c)** Polarization map of the active region that is highly left polarized with a maximum degree greater than 90% at this time. **d)** Magnetogram of the region with $|B|_{\max} = 3358$ G.

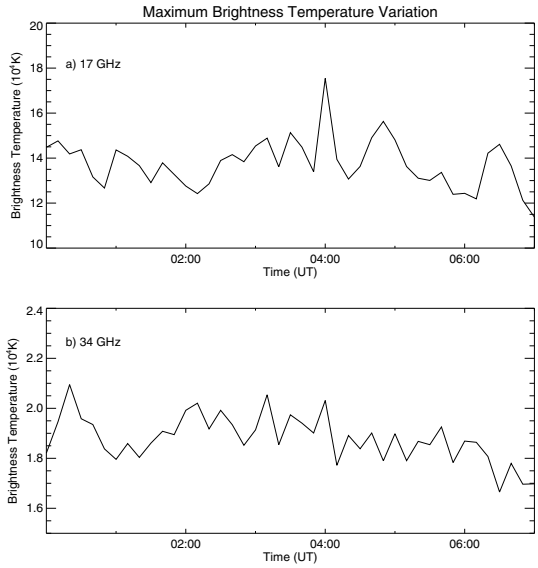

Fig. 2. Temporal variation of the maximum brightness temperature **a)** 17 GHz and **b)** 34 GHz.

(Sakurai 1989; Mandrini et al. 2000; Régnier et al. 2002; Jain & Mandrini 2006).

The main goal of this work is to make a 3D atmospheric model, by calculating the brightness temperature at radio frequencies to reproduce the NoRH observations of active regions at 17 GHz and 34 GHz. The next section summarizes the observations. The atmospheric model is described in Sect. 3, which includes the magnetic field extrapolation (3.1), changes in the quiet Sun density and temperature distributions (3.2), and the brightness temperature calculations (3.3). The results are described and discussed in Sect. 4. The main conclusions of this work are summarized in Sect. 5.

2. Observations

The NoRH has been observing the Sun routinely at 17 GHz since 1992 and produces 10–18 arcsec resolution images of intensity and polarization (right and lefthand), and intensity maps at 34 GHz after 1996 with 5–10″ spatial resolution. In this work, we studied a stable active region close to the solar disk center, observed between 0:00:00 and 7:00:00 UT on 2002 June 25 (NOAA 10008) at both frequencies. The time interval between each NoRH map used here is 10 min.

We also used magnetograms observed by MDI (Michelson Doppler Imager) onboard the SOHO (SOlar and Heliospheric Observatory) satellite to extrapolate the atmospheric magnetic field (Scherrer et al. 1995). This is discussed in the next section.

Figure 1a shows the selected active region at 17 GHz with an area of approximately 500×500 arcsec^2. Figure 1b presents the same region in detail with brightness temperature curves of 1.3, 2.5, 5.0, and 10.0×10^4 K. Figures 1c and d show a polarization map of the same region at 17 GHz and its MDI magnetogram, respectively. At this time the region had its lefthand polarization maximum greater than 90%, whereas the magnetogram presented a maximum magnetic field intensity of $|B|_{\max} = 3358$ G. The MDI magnetogram used is close in time with the NoRH images, as can be seen by the times shown on the top of each image.

Even though there were no flaring events observed during this observation time, this active region was highly left-circular polarized with a mean maximum degree of polarization of $85 \pm 5\%$ during the day. The brightness maximum temperature at 17 GHz varied from 1.14×10^5 K (7:00:00 UT) to 1.76×10^5 K (4:00:00 UT) at 17 GHz, and from 1.7×10^4 K (6:30:00 UT) to 2.1×10^4 K (0:20:00 UT) at 34 GHz. Figure 2 shows the maximum brightness temperature variation at 17 GHz and 34 GHz.

3. 3D atmospheric model

3.1. Magnetic field extrapolation

The extrapolation of the magnetic field lines above the photosphere/chromosphere is the main tool for topological reconstruction of the magnetic field. Justified by a small plasma beta in active regions, a reasonable assumption for the magnetic field results from the theory of force-free current-carrying fields. Magnetograms can be used in a boundary value problem for the main law of the force-free fields

$$\nabla \times \boldsymbol{B} = \alpha \boldsymbol{B}.$$

An assumption that is often adopted is constant alpha across the lines, which makes the solution of this equation linear. To solve it numerically, different methods have been used (e.g. McClymont et al. 1997). The great advantage in using the linear force-free field solution is the use of the LOS (line-of-sight) magnetogram, such as the high-resolution MDI observations. Depending on how the boundary value region is related to the whole volume, two slightly different solutions may be obtained (Nakagawa & Raadu 1972; Seehafer 1978).

Imaging of atmospheric plasma such as EUV observations provide a two-dimensional (2D) projection of topological aspects of the field lines at coronal level. The free alpha parameter is then chosen by the best match with EUV loop patterns.

Following Nakagawa & Raadu (1972), we have developed a computational program for potential $\alpha = 0$ and linear force-free field extrapolation from line-of-sight magnetograms. The

selected area of the solar disk that includes the active region (NOAA 10008) in the magnetogram has 256×256 pixel^2 (about 500×500 arcsec^2). This base 2^x was chosen for a faster computing process, and the cube height is 100 arcsec (200 arcsec).

3.2. Densities and temperature distributions

The presence of a magnetic field changes the atmospheric distribution of particle (electrons and ions) densities and temperatures. In this work, we extended the SSC (Selhorst et al. 2005b) quiet Sun model up to an atmospheric height of 1.5×10^5 km and used its density and temperature distributions for the atmosphere surrounding the active region. We propose that the active region volume is defined by those magnetic flux tubes anchored at photospheric level by magnetic fields higher than some threshold, for example, $|B| > 1000$ G, and are responsible for the changes in the quiet atmosphere above.

The cube with the magnetic field extrapolation provides the 3-component (B_x, B_y, B_z) positions of magnetic field lines. Since the photosphere is optically thick for radio emission, in our model we consider that the temperature and densities distributions within the flux tubes only differ from the quiet Sun values above 1000 km, that is, well above the photosphere. We also propose a flux tube temperature distribution in the chromosphere with a linear increase with height ($\nabla T > 0$), whereas the particle density decreases with a negative gradient (∇n_e) in that region. In the transition region and corona, the temperature and density distributions are greater than the quiet Sun by constant values, N_T and N_{n_e}:

$$N_T = \frac{T_{AR}}{T_{qS}} \text{ and } N_{n_e} = \frac{n_{e_{AR}}}{n_{e_{qS}}}$$

where T_{qS} and $n_{e_{qS}}$ are the temperature and density in the quiet Sun atmosphere, respectively, and T_{AR} and $n_{e_{AR}}$ are the active region counterpart.

Fontenla et al. (1993) proposed that over typical plages the coronal heating extends to deeper levels in the atmosphere in comparison to the average quiet Sun regions, which results in a lower transition region. Following this suggestion, we propose that the transition region over the active region are located at 3000 km above the surface, about 500 km below its height in a quiet Sun region.

Figure 3a shows the quiet Sun temperature distribution (SSC model) and an example of the temperature distribution in the flux tube. In this example, the chromospheric temperature in the flux tube has a gradient of $\nabla T = 7.08$ K km^{-1}. The temperature distribution above the transition region is 10 times greater than the quiet Sun temperature ($N_T = 10$). With respect to the density distribution, the example in Fig. 3b shows a flux tube with $\nabla_{n_e} = -3.97 \times 10^7$ cm^{-3} km^{-1} in the chromosphere and an increment ratio $N_{n_e} = 4$ in the transition region and corona.

3.3. Total brightness temperature

Total brightness temperature was estimated by computing the radiative transfer by integrating in height within the solar atmosphere. This is done along each cube column, taking into consideration the values of density, temperature, and magnetic field intensity for each point. The spatial resolution along the column was 50 km, which results in an integration of nearly 3000 points. This distance resolution is important mainly between 2500 and 5000 km, due to the strong variation in the physical parameters where the upper chromosphere and the transition region are located in the model and where most of the 17 GHz emission originates from.

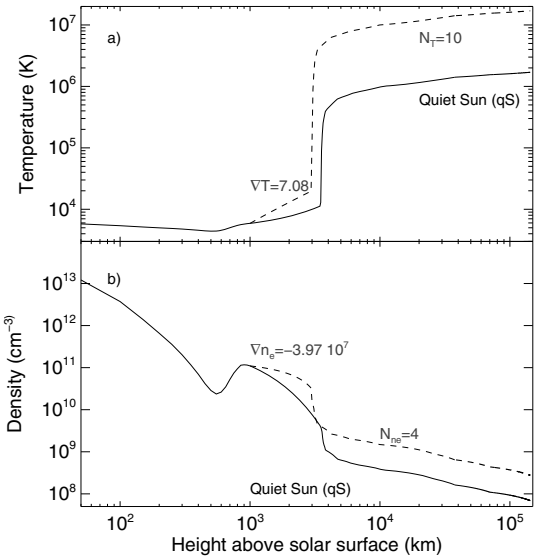

Fig. 3. Comparison between the quiet Sun atmosphere (solid line) and active region atmosphere (dashed line) for temperature **a)** and density **b)** distributions.

Here we have employed the equations deduced by Dulk (1985) for calculating the absorption coefficient for bremsstrahlung and gyro-resonance emission of thermal electrons. The total absorption coefficient is assumed to be the sum of both coefficients. For a fast computational result, gyro-resonance absorption coefficient is only calculated for harmonics smaller than 5, because the contribution of higher harmonics to the 17 GHz emission is very small (Shibasaki et al. 1994).

4. Results

The magnetograms used in this work were re-calibrated by the MDI team (after October 2007) which increased the intensity in the magnetograms by a factor of approximately 1.7 when compared with previous data. The active region NOAA 10008 presented a maximum magnetic field of $|B| = 3400 \pm 340$ G at the photosphere, which is consistent with magnetic field intensities of $|B| \sim 2000$ G at chromospheric/transition region heights, which is able to produce gyro-resonance emission at the 17 GHz third harmonic.

Despite the intensity correction, the MDI magnetograms still have the problem of saturated points (Liu & Norton 2006; Livingston et al. 2006). The NOAA 10008 magnetogram presented at least 8 points in the intense negative area (2 points per line) with clear saturation. To minimize this problem, we made a linear interpolation between the non-saturated points. Even though the number of saturated points is small, the magnetic field extrapolations are completely modified and the resulting brightness temperature underestimated resulting in temperatures 30–40% smaller in the worst cases. Figure 4 shows an example of this procedure.

Figure 5 shows the variation in the total absorption coefficient and the opacity as a function of height above the solar photosphere at 17 GHz. In the example presented in Fig. 5, we used a potential extrapolation of the magnetogram modified by the linear corrections. In this scenario, the third harmonic is generated close to the transition region.

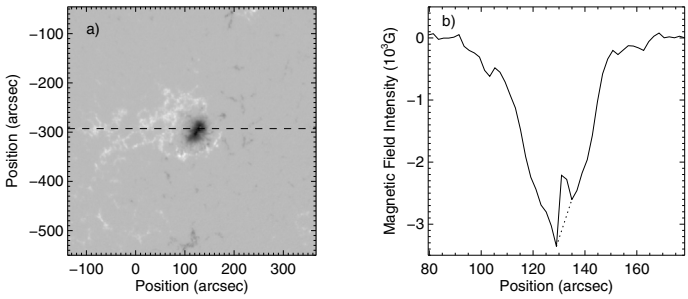

Fig. 4. a) NOAA 10008 magnetogram. The dashed line cross over saturated points in the magnetogram. **b)** The magnetic field intensity profile across the dashed line in Fig. 4a showing the saturated points and the linear correction proposed here (dotted line).

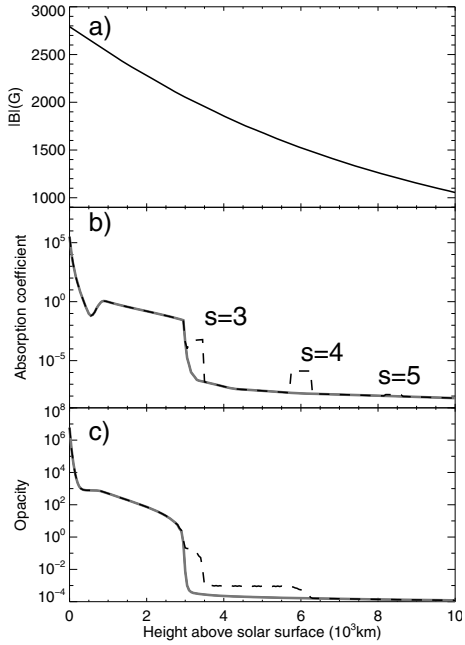

Fig. 5. Distribution of **a)** magnetic field intensity, **b)** absorption coefficient, and **c)** opacity with the height above the solar surface at the position where the simulation brightness temperature at 17 GHz reaches its maximum value. The gray line represents the emission due only to free-free emission, whereas the black dashed lines show the gyro-resonance plus the free-free emission.

The dominance of the third harmonic with respect to higher harmonics of gyro-resonance emission at 17 GHz is clearly seen in Fig. 5. The opacity in the region of the third harmonic formation increased from 10^{-4} to 10^{-1}, whereas in the region of the fourth harmonic formation, the opacity increased less than one order of magnitude with respect to the free-free opacity.

At 34 GHz, the maximum absorption coefficient due to gyro-resonance emission occurs in the harmonic six; however, it is 5 orders of magnitude smaller than the absorption coefficient due to free-free emission, so its influence on the total brightness temperature can be neglected.

Table 1 presents 18 simulations where all extrapolated magnetic field lines with photospheric intensities greater than 1000 G generated a flux tube around them. This procedure resulted in a total of 325 flux tubes. All flux tubes had a width of 4500 km and density and temperature distributions distinct from the quiet Sun values. Each simulation in Table 1 has a different distribution of density and temperature within the flux tubes. The last two columns present the resulting maximum brightness temperatures at 17 and 34 GHz, respectively. These simulations were all compatible with the maximum brightness temperatures observed in active region NOAA 10008 on June 25, 2002.

The resulting maximum brightness temperatures for potential extrapolation ($\alpha = 0$) presented in Table 1 vary from 0.89×10^5 to 2.33×10^5 K at 17 GHz, whereas the variation at 34 GHz was very small, ranging between 0.15×10^5 and 0.21×10^5 K. The brightness temperature at 17 GHz is more dependent on the coronal temperature since the greatest emission originates from gyro-resonance due to the third harmonic, which is formed close to the transition region (see Fig. 5). On the other hand, changes at coronal heights do not affect the emission at 34 GHz, which is caused totally by the thermal bremsstrahlung produced in the chromosphere.

It can be seen from Fig. 5 that the third harmonic at 17 GHz occurs at the base of the corona (3000–3500 km). In this region, the local temperature is about 10–12 times the coronal temperature in quiet Sun, which yields coronal temperatures of $4–5 \times 10^6$ K within the magnetic flux tubes at 3500 km above the solar surface. The lower temperature is consistent with the quiescent component for active regions observed in soft X-rays; however, the upper temperature limit in our simulations is close to the lower limit for coronal hot transient components proposed by Yoshida & Tsuneta (1996).

Using EUV data (171 and 195 Å) from the TRACE (Transition Region And Coronal Explorer) satellite Testa et al. (2002), found evidence of high temperature fibrils in active regions ($T \sim 5 \times 10^6$ K). The authors used an extended approach for the TRACE temperature response function ranging from 10^5 to 10^7 K, while the standard approach considers only temperatures between 0.9 and 1.8×10^6 K (Aschwanden et al. 2000; Lenz et al. 1999). Moreover Reale & Peres (2000), suggest that the coronal loops observed with TRACE are composed of unresolved fine structures with a great range of temperatures ($0.8–5.0 \times 10^6$ K). These results agree with the range of temperatures necessary for our active region model.

The influence of magnetic field shear in the 17 GHz brightness temperature was tested in the simulations 10–18 in Table 1. The simulations show that the maximum brightness temperature was reduced by the α increase, and this reduction was approximately 10% between a potential extrapolation and a force-free field extrapolation with $\alpha = 1.10 \times 10^{-2}$ Mm^{-1}. Only positive values of α were tested because negative values shear the magnetic field in the counterclockwise direction, which is opposite to the inclination in the observed 17 GHz map (see Fig. 6a).

In Fig. 6 we compare the brightness temperature distribution between the observation at 17 GHz (panel a) and potential (panel b) and force-free simulations with positive α (panels c and d). At the time of observation, the maximum brightness temperature was 1.49×10^5 K, which is close to the maximum obtained in the simulations presented in simulation 14 of Table 1, $1.40–1.52 \times 10^5$ K. The brightness temperature maximum also occurs at the same position; however, the core region with temperatures above 10^5 K has a different tilt than the simulation. Moreover, the region of lower temperatures ($<0.15 \times 10^5$ K), where only the thermal bremsstrahlung is important, has approximately the same area both in the simulations and the observed active region. However, the shape has small differences when compared with the observation. Probably these differences are due to the number of flux tubes and their width, which change the lower atmosphere in which the bremsstrahlung emission is formed.

The inclination of the simulated hot source does not present visible changes because of the shear in the magnetic field lines,

Table 1. Maximum brightness temperatures at 17 and 34 GHz resulting from the NOAA 10008 simulations and their free parameters.

	∇T (K km^{-1})	N_T	∇n_e (cm^{-3} km^{-1})	N_{n_e}	$T_{B_{max}}$ ($\times 10^5$ K)			
					17 GHz			34 GHz
			$\alpha =$ ($\times 10^{-2}$ Mm^{-1})		0.00	0.70	1.10	0.00
1	4.56	10	–4.38	3	0.89	–	–	0.15
2	4.56	11	–4.38	3	1.14	–	–	0.15
3	4.56	12	–4.38	3	1.43	–	–	0.15
4	4.56	10	–3.97	4	1.15	–	–	0.15
5	4.56	11	–3.97	4	1.48	–	–	0.15
6	4.56	12	–3.97	4	1.87	–	–	0.15
7	4.56	10	–3.55	5	1.42	–	–	0.16
8	4.56	11	–3.55	5	1.81	–	–	0.16
9	4.56	12	–3.55	5	2.29	–	–	0.16
10	7.08	10	–4.38	3	0.94	0.90	0.87	0.19
11	7.08	11	–4.38	3	1.18	1.13	1.09	0.19
12	7.08	12	–4.38	3	1.48	1.41	1.36	0.19
13	7.08	10	–3.97	4	1.19	1.14	1.10	0.20
14	7.08	11	–3.97	4	1.52	1.45	1.40	0.20
15	7.08	12	–3.97	4	1.90	1.82	1.75	0.20
16	7.08	10	–3.55	5	1.46	1.40	1.35	0.21
17	7.08	11	–3.55	5	1.85	1.77	1.71	0.21
18	7.08	12	–3.55	5	2.33	2.23	2.14	0.21

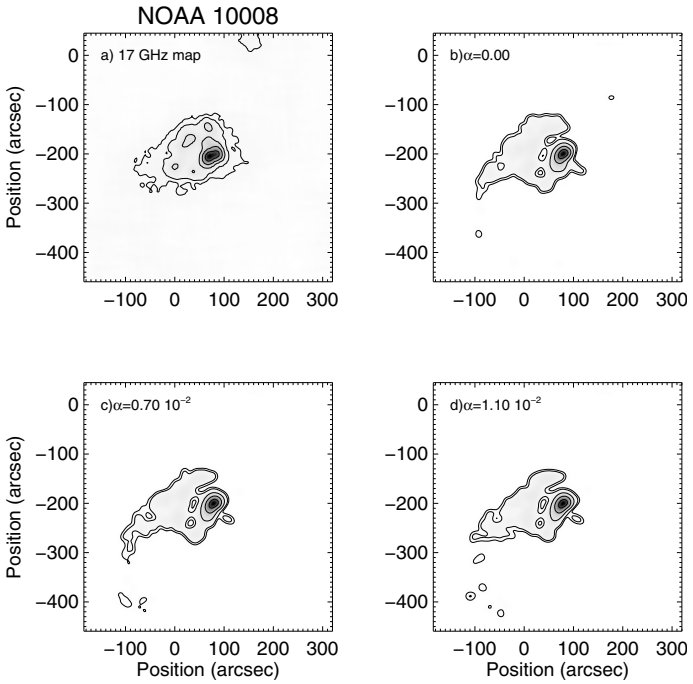

Fig. 6. a) Active region NOAA 10008 observed at 03:10:00 UT at 17 GHz. Model simulation with different α parameters are presented in: **b)** $\alpha = 0.00$, **c)** $\alpha = 0.70 \times 10^{-2}$, and **d)** $\alpha = 1.10 \times 10^{-2}$ Mm^{-1}. All images display brightness temperature contours of 0.13, 0.15, 0.25, 0.50, and 1.00×10^5 K with a negative color scale.

which could reflect the concentration of intense and almost vertical magnetic field lines. To change their inclination with a single α we would need to increase its value to unrealistic ones.

5. Conclusions

The goal of this work is to model the emission of an active region with strong gyro-resonance and bremsstrahlung at radio wavelengths, in order to reproduce the observations at 17 and 34 GHz obtained by the NoRH.

We chose a highly polarized active region at 17 GHz (NOAA 10008) to test the model. This region presented maximum brightness temperature above 10^5 K and a maximum degree of polarization over 70% at 17 GHz on 2002 June 25. Following Vourlidas et al. (2006) and Shibasaki et al. (1994), we proposed that gyro-resonance emission at 17 GHz originates from the third harmonic (~2000 G). However, the early MDI magnetograms (before October 2007) were not able to measure magnetic field values above ~2000 G (Liu & Norton 2006; Livingston et al. 2006), which makes the generation of 17 GHz impossible by the third harmonic in the solar atmosphere. After October 2007, the MDI team re-calibrated all magnetograms increasing its intensity by a factor of approximately 1.7 in relation to the previous data. Despite the intensity correction, the problem with saturated points in the MDI magnetograms still persists.

The active region studied here (NOAA 10008) presented a maximum magnetic field of $|B| = 3400 \pm 340$ G at the photosphere; however, it presented at least 8 saturated points in the intense negative area (2 points per line). To minimize this problem, we applied a linear interpolation between the unsaturated points (Fig. 4). This simple correction increased by about 50% the maximum brightness temperatures in our model simulations.

Following the proposition of Fontenla et al. (1993) for solar atmosphere over plages, we suggest that the transition region over the active region starts about 500 km below its height in the atmosphere over a quiet Sun region.

The magnetic field extrapolation from magnetograms yields gyro-resonance emission at the third harmonic emission close to the coronal base (3000–3500 km). To reproduce the brightness temperature observed at 17 GHz ($1.14–1.74 \times 10^5$ K), the local temperature in the flux tubes used ranged from 4 to 5×10^6 K. These high temperatures agree with the temperatures proposed by Yoshida & Tsuneta (1996) for the quiescent (lower limit) and transient components (upper limit) observed in soft X-rays. A transient component of high temperature is able to explain the fast increase in the maximum brightness temperature values at

17 GHz, for example, the maximum brightness temperature observed at 4:00:00 UT (Fig. 2).

We conclude from the spatial brightness temperature distribution that the emission of active region NOAA 10008 at 17 GHz is reproduced by potential or force-free magnetic field extrapolations with low positive α (0.70–1.10×10^{-2} Mm^{-1}). The difference between the potential and force-free simulation is very small, especially within the hot source, where the emission is dominated by gyro-resonance. This could be explained by the magnetic field lines being approximately vertical and located very high above the strong negative region. Moreover, the heights reached in the solar atmosphere due to the choice of minimum magnetic field lines footpoints (1000 G) resulted in slight changes in the low brightness region, that is dominated by the bremsstrahlung emission.

In conclusion, the active region atmospheric model proposed here is able to reproduce the brightness temperatures observed at radio frequencies when considering both the bremsstrahlung and gyro-resonance emission mechanisms.

Acknowledgements. The authors would like to thank the Nobeyama Radioheliograph, which is operated by the NAOJ/Nobeyama Solar Radio Observatory. SOHO is a project of international collaboration between ESA and NASA. C.L.S. thanks Dr. Kiyoto Shibasaki and the NoRH staff for the opportunity to work at Nobeyama for two months.

References

Aschwanden, M. J., Nightingale, R. W., & Alexander, D. 2000, ApJ, 541, 1059
Dulk, G. A. 1985, ARA&A, 23, 169
Fontenla, J. M., Avrett, E. H., & Loeser, R. 1993, ApJ, 406, 319
Jain, R. & Mandrini, C. H. 2006, A&A, 450, 375
Kundu, M. R., White, S. M., Shibasaki, K., & Raulin, J.-P. 2001, ApJS, 133, 467
Lenz, D. D., Deluca, E. E., Golub, L., Rosner, R., & Bookbinder, J. A. 1999, ApJ, 517, L155
Liu, Y. & Norton, A. A. 2006, in AAS/Solar Physics Division Meeting, 07.15
Livingston, W., Harvey, J. W., Malanushenko, O. V., & Webster, L. 2006, Sol. Phys., 239, 41
Mandrini, C. H., Démoulin, P., & Klimchuk, J. A. 2000, ApJ, 530, 999
McClymont, A. N., Jiao, L., & Mikic, Z. 1997, Sol. Phys., 174, 191
Nakagawa, Y., & Raadu, M. A. 1972, Sol. Phys., 25, 127
Nakajima, H., Nishio, M., & Enome, S., E. A. 1994, Proc. IEEE, 82, 705
Reale, F., & Peres, G. 2000, ApJ, 528, L45
Régnier, S., Amari, T., & Kersalé, E. 2002, A&A, 392, 1119
Sakurai, T. 1989, Space Sci. Rev., 51, 11
Scherrer, P. H., Bogart, R. S., Bush, R. I., et al. 1995, Sol. Phys., 162, 129
Seehafer, N. 1978, Sol. Phys., 58, 215
Selhorst, C. L., Costa, J. E. R., & Silva, A. V. R. 2005a, in ESA SP-600, The Dynamic Sun: Challenges for Theory and Observations
Selhorst, C. L., Silva, A. V. R., & Costa, J. E. R. 2005b, A&A, 433, 365
Shibasaki, K., Enome, S., Nakajima, H., et al. 1994, PASJ, 46, L17
Testa, P., Peres, G., Reale, F., & Orlando, S. 2002, ApJ, 580, 1159
Vourlidas, A., Gary, D. E., & Shibasaki, K. 2006, PASJ, 58, 11
White, S. M., Kundu, M. R., Shimizu, T., Shibasaki, K., & Enome, S. 1995, ApJ, 450, 435
Yoshida, T. & Tsuneta, S. 1996, ApJ, 459, 342